Influence of Third Harmonic Injection on MMC-based HVDC Transmission Systems

Rui Li[1], John E. Fletcher[2], and Barry W. Williams[1]

[1]Department of Electronic and Electrical Engineering, University of Strathclyde, Glasgow, UK

[2]School of Electrical Engineering and Telecommunications, University of New South Wales, Sydney, Australia

E-mail: rui.li@strath.ac.uk

***Abstract*—**Whilst third harmonic injection is extensively used in modular multilevel converter (MMC) control, its significant advantages over sinusoidal modulation have not been fully explored. This paper evaluates the influence of third harmonic injection on system power losses, submodule capacitance, circulating current, and fault current and mathematical models are derived. Station conduction losses are reduced by 11%, yielding higher efficiency and lowering cooling system capacity. The submodule capacitance is reduced by 24%, which significantly lowers the capital cost, weight, and volume of the station converter. Additionally, the phase energy variation is reduced by around 18%, which benefits circulating current control. Due to the lower AC currents, the semiconductor current stresses are correspondingly reduced. In addition to the performance improvement in normal operation, the third harmonic injection reduces the DC fault currents by 13.4% and thus the fault current stresses on semiconductors and DC circuit breakers are lowered. Simulation of a point-to-point HVDC system demonstrates the effectiveness of the above analysis.

***Index Terms*—**DC fault current, HVDC transmission, modular multilevel converter (MMC), power loss, submodule capacitance, third harmonic injection.

I. INTRODUCTION

Modular multilevel converter (MMC) deployment for HVDC transmission applications is increasing due to its advantages over thyristor-based line commutated converters (LCCs) and two-level voltage source converters (VSCs). A three-phase transformer is used on the MMC AC-side to isolate the grid and the converter and match the AC and DC voltages. Thus sinusoidal modulation can generate the required voltage and control the MMC, although the DC voltage is not fully utilised. Additionally, it has good harmonic characteristics and can be simply implemented in digital controllers. As a result, sinusoidal modulation is widely used in the control of MMCs [1-3].

Selective harmonic elimination (SHE) modulation is introduced in [4] to control the hybrid multilevel converter and reduce switching losses. However, the active switches of the main power stage still suffer high voltage stresses. Trapezoidal modulation is utilized in the solid-state DC transformer and in the hybrid cascaded MMC in [5] and [6] respectively to reduce switching losses and effectively utilize the DC voltage to produce an output AC voltage with higher fundamental amplitude. However, this is achieved at the expense of higher capital cost and a larger footprint.

By adding zero-sequence components into the reference voltage, the discontinuous modulation in [7, 8] increases the modulation gain and reduces switching losses. However, additional submodules (SMs) are required in each arm to avoid over-modulation and reduce SM capacitor voltage ripple. In [9], second harmonic is injected into arm currents to optimize the current distribution among the SMs and reduce SM capacitor voltage ripple, but at the expense of higher semiconductor current stresses.

Third harmonic injection is another attractive approach for MMC control, due to the high DC voltage utilization ratio. In [10], the MMC was first proposed for high voltage application and triplen harmonics, mainly third harmonic, were injected to effectively utilize the DC voltage. The advantage of third harmonic injection over sinusoidal modulation is discussed in [11] and the system performance under a DC fault is improved. However, the influence of third harmonic during normal operation is not considered.

MMC dynamics under both balanced and unbalanced grid conditions with third harmonic injection are evaluated in [12]. However, the influence of the third harmonic on

losses and SM capacitance is not considered. Modified space-vector (SV) nearest level modulation (NLM) is discussed in [13] to increase the DC voltage utilization ratio thus reduce the DC voltage. However, the reduced DC voltage means a higher DC current in order to transfer rated power, resulting in higher power transmission losses.

Although third harmonic injection is extensively used in MMC control, its advantages over sinusoidal modulation have not been fully exploited in the MMC [10-13]. By injecting the triplen harmonics, the DC voltage utilization ratio is increased from ½ to $1/\sqrt{3}$ [7, 14]. Compared with sinusoidal modulation, the maximum output voltage peak with reference to the mid-point of the DC link is reduced from $½V_{DC}$ to $¼\sqrt{3}V_{DC}$ as demonstrated in Fig. 1 (a), while the amplitude of the output fundamental voltage remains $½V_{DC}$, where V_{DC} is the DC voltage. For simplicity, it is assumed that $½\sqrt{3}N$ is an integer, where N is the SM number per arm. Only $½\sqrt{3}N$ of the SMs are utilized when third harmonic injection is used rather than sinusoidal modulation. In real application, the potentially used SMs are $ceil\left(½\sqrt{3}N\right)$, which is close to $½\sqrt{3}N$ given that HVDC systems typically use hundreds of SMs per arm.

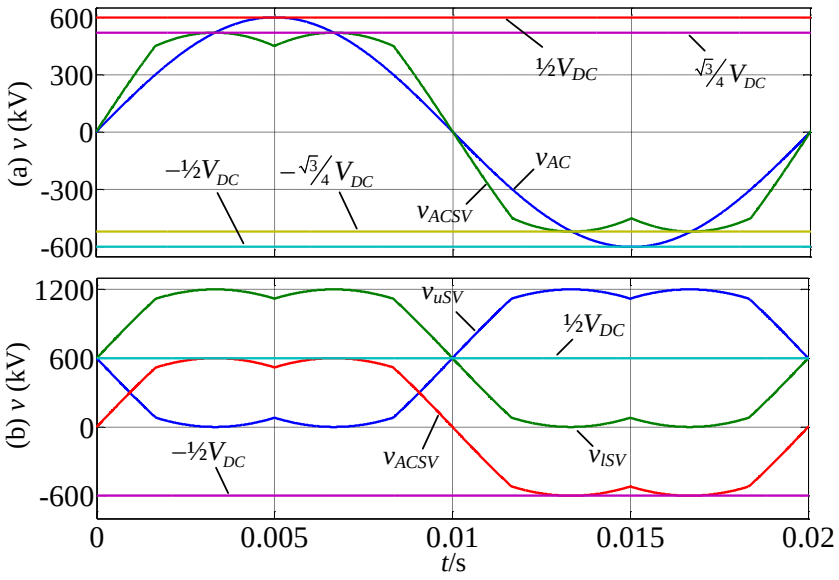

Fig. 1. Reference voltages: (a) comparison between sinusoidal modulation and third harmonic injection, where m_0=1, m_{SV} =½$\sqrt{3}$ and V_{DC}=1200 kV and (b) third harmonic injection with higher transformer ratio, where m_{SV}=1 and V_{DC}=1200 kV.

In HVDC systems, by increasing the transformer ratio between the converter-side and the grid-side by 15.5%, higher voltage is induced on the converter-side of the transformer,

when the voltage of the grid connected to the station remains unchanged. Thus, higher voltage output capability is required for the MMC and the redundant SMs, introduced by the higher DC voltage utilization capability with third harmonic injection, can be effectively utilized.

This study focuses on the influence of third harmonic injection on SM capacitance, converter losses, circulating currents, and DC fault currents, in a HVDC system. The paper is organized as follows. The characteristics of third harmonic injection with higher transformer ratio are presented in Sections II. In Section III, the influence of third harmonic injection on station conduction losses, SM capacitance requirements, circulating currents, and DC fault currents are discussed and mathematical models are derived. In Section IV, system performances using third harmonic injection are assessed in normal operation and during a pole-to-pole DC fault, by considering a point-to-point HVDC link. Finally Section V draws the conclusions.

II. Characteristics of Third Harmonic Injection with Higher Transformer Ratio

In this paper, third harmonic is injected into the three phase sinusoidal voltages v_a, v_b, and v_c by

$$\begin{cases} v_{aSV} = v_a - v_{hSV} \\ v_{bSV} = v_b - v_{hSV} \\ v_{cSV} = v_c - v_{hSV} \end{cases} \tag{1}$$

where v_{aSV}, v_{bSV}, and v_{cSV} are the three phase voltages with third harmonic, referenced to the mid-point of the DC link, and

$$v_{hSV} = \tfrac{1}{2}\left[\max\left(v_a, v_b, v_c\right) + \min\left(v_a, v_b, v_c\right)\right]. \tag{2}$$

Besides the third harmonic, the voltage v_{hSV} contains other triplen harmonics. However, the third harmonic is the dominant frequency in the triplen harmonics and the influence of other triplen harmonics (h=9th, 15th, …) is ignored (purely third harmonic injection is a valid concept for increasing the DC voltage utilization ratio by 15.5%). The adopted third harmonic injection approach described by (1) and (2) has the same effect as space-vector modulation, as presented in [12, 14, 15]. Moreover, it is easy to implement and does not cause extra computational burden for the controller, even for MMC with several hundred SMs per arm.

By using the third harmonic injection with a higher transformer ratio, the maximum output voltage peak is increased to $½V_{DC}$, thus the modulation index is increased from $½\sqrt{3}$ to 1 and all the SMs are effectively utilized, as shown in Fig. 1 (b).

As the transferred power is fixed, the AC current i_{ACSV} is reduced by 13.4%:

$$i_{ACSV} = ½\sqrt{3} I_{m0} \sin(\omega t - \varphi) \tag{3}$$

where I_{m0} is the AC current amplitude in sinusoidal modulation control; ω is the grid angular velocity; and φ is the phase angle between the phase voltage and current. As depicted in [16], the AC current amplitude I_{m0} can be expressed in terms of the DC current i_{DC}, then (3) can be rewritten as

$$i_{ACSV} = \frac{\sqrt{3}}{2} \frac{4 i_{DC}}{3 m_0 \cos\varphi} \sin(\omega t - \varphi) = \frac{2\sqrt{3} i_{DC}}{3 m_0 \cos\varphi} \sin(\omega t - \varphi) \tag{4}$$

where m_0 is the modulation index with sinusoidal modulation.

III. Influence of Third Harmonic Injection on MMCs

In this section, the influences of third harmonic injection with a resultant higher transformer ratio are discussed in normal operation and during pole-to-pole DC fault, respectively.

A. Power Losses

The conduction losses are higher than the switching losses in MMCs for HVDC application and are the dominant part of station converter losses. Thus, only the conduction losses are discussed. Considering the DC and fundamental frequency components, the upper and lower arm currents are described as:

$$i_{uSV} = ⅓ i_{DC} + ½ i_{ACSV} = ⅓ i_{DC} \left[1 + \frac{\sqrt{3} \sin(\omega t - \varphi)}{m_0 \cos\varphi} \right] \tag{5}$$

$$i_{lSV} = ⅓ i_{DC} - ½ i_{ACSV} = ⅓ i_{DC} \left[1 - \frac{\sqrt{3} \sin(\omega t - \varphi)}{m_0 \cos\varphi} \right]. \tag{6}$$

For simplicity, the forward voltages of the IGBT and freewheel diode are assumed to be identical and independent to the current flowing through the semiconductors. This simplification significantly reduces the calculation complexity compared to the approach as presented in [17, 18] and is adopted in this study to evaluate the influence of the third harmonic injection on the station converter conduction losses. As the semiconductor number in the current path per arm is *N*, according to (5), the station converter conduction loss can be calculated as:

$$\begin{aligned} P_{lossSV} &= \frac{6}{2\pi}\int_0^{2\pi} NV_{fd}\left|i_{uSV}\right| d(\omega t) \\ &= \frac{4NV_{fd}i_{DC}}{\pi}\left(\frac{\sqrt{3-m_0^{\,2}\cos^2\varphi}}{m_0\cos\varphi}+\arccos\sqrt{1-\tfrac{1}{3}m_0^{\,2}\cos^2\varphi}\right) \end{aligned} \tag{7}$$

where V_{fd} is the simplified forward voltages of the IGBT and freewheel diode. Similarly, the conduction loss of the station converter with the sinusoidal modulation is:

$$P_{loss0} = \frac{4NV_{fd}i_{DC}}{\pi}\left(\frac{\sqrt{4-m_0^{\,2}\cos^2\varphi}}{m_0\cos\varphi}+\arccos\sqrt{1-\tfrac{1}{4}m_0^{\,2}\cos^2\varphi}\right). \tag{8}$$

As the circulating current can be controlled around zero by proportional-resonant (PR) control, its influence on conduction losses are slight, and not accounted for in (7) and (8).

A station converter with parameters listed in Table I is tested. To reduce model complexity, the SM number per arm *N* is reduced and chosen as 24 with half-bridge (HB) SMs operating at 50 kV. In typical applications, hundreds of submodules with voltage rating of several kilovolts are required, however from a simulation perspective, assuming the adopted model with reduced SMs accelerates simulation time but does not significantly affect the quality of the outcome [6, 16, 19].

In the detailed switching model, the IGBTs (including the anti-parallel diodes) are modelled by the Universal Bridge Block in the MATLAB/Simulink® environment. Each SM in the tested model represents several tens of series-connected SMs of a practical implementation [19]. The parameters of the IGBTs and diodes are thus required to be set according to the equivalent series-connected circuit. With the detailed parameters as listed in Table II, the conduction power losses of the test station with sinusoidal modulation and third

harmonic injection are, from (8) and (7):

$$P_{loss0} = 10.8 \text{ MW}, \qquad P_{lossSV} = 9.6 \text{ MW}. \tag{9}$$

Compared with sinusoidal modulation, the station conduction losses with third harmonic injection are reduced by 11%. This significantly reduces station conduction losses, yielding higher efficiency and a reduced capacity cooling system. The above calculated conduction losses are in agreement with that obtained by simulation, as presented in [17, 18].

TABLE I

Comparison between Sinusoidal Modulation and Third Harmonic Injection

PARAMETER	Sinusoidal modulation	Third harmonic injection
AC grid voltage	480 kV	
Power rating	1650 MW	
DC voltage V_{DC}	1200 kV	
Arm inductance	0.05 pu	
Modulation index m_0	0.8	
Number of SMs per arm N	24	
SM capacitance	334 μF	
SM capacitor voltage	50 kV	
SM capacitor voltage ripple	±8.4%	**±6.4%**
Arm current peak	1600 A	**1450 A**
Induced voltage on converter-side of transformer	590 kV	**680 kV**
Converter-side current of transformer	1620 A	**1400 A**
Station conduction loss	P_{loss0}	$\mathbf{0.89}\boldsymbol{P_{loss0}}$
DC fault current	i_{fc0}	$\mathbf{0.866}\boldsymbol{i_{fc0}}$

TABLE II

Parameters of the Tested Model with Reduced SMs for Conduction Loss Calculation.

SM number per arm N	DC current i_{DC}	Forward voltages V_{fd}	Modulation index m_0	Phase angle φ
24	1.375 kA	95 V	0.8	0

B. SM Capacitance Requirements

The specified maximum capacitor voltage ripple typically determines the SM

capacitance requirement [20]. This section presents the process of sizing the capacitances for the MMC with third harmonic injection.

Due to the third harmonic, the converter can generate higher fundamental voltage than with sinusoidal modulation:

$$v_{ACSV} = \frac{V_{DC}}{\sqrt{3}}\left[m_0 \sin \omega t + m_{hSV} \sin 3\omega t\right] \tag{10}$$

where m_{hSV} is the modulation index of third harmonic voltage. From (10), the upper and lower arm voltages are expressed as

$$v_{uSV} = \tfrac{1}{2}V_{DC}\left[1 - \frac{2}{\sqrt{3}} m_0 \sin \omega t - \frac{2}{\sqrt{3}} m_{hSV} \sin 3\omega t\right] \tag{11}$$

$$v_{lSV} = \tfrac{1}{2}V_{DC}\left[1 + \frac{2}{\sqrt{3}} m_0 \sin \omega t + \frac{2}{\sqrt{3}} m_{hSV} \sin 3\omega t\right]. \tag{12}$$

From (5), (6), (11), and (12), integrating the arm voltage multiplied by the arm current, the upper and lower arm energy variations are

$$\Delta E_{uSV}(\omega t) = \frac{1}{\omega}\int_0^{\omega t} v_{uSV} i_{uSV} d(\omega t) =$$
$$\frac{V_{DC} i_{DC}}{6\omega}\left\{-\frac{\sqrt{3}}{m_0 \cos\varphi}\left[\cos(\omega t - \varphi) - \cos\varphi\right] + \frac{2}{\sqrt{3}} m_0\left[\cos(\omega t) - 1\right] + \frac{1}{2\cos\varphi}\left[\sin(2\omega t - \varphi) + \sin\varphi\right]\right\} \tag{13}$$
$$-\frac{m_{hSV} V_{DC} i_{DC}}{3\sqrt{3}\omega}\left\{-\frac{\cos(3\omega t) - 1}{3} + \frac{\sqrt{3}}{2m_0 \cos\varphi}\left[\tfrac{1}{2}\sin(2\omega t + \varphi) - \tfrac{1}{4}\sin(4\omega t - \varphi) - \tfrac{3}{4}\sin\varphi\right]\right\}$$

$$\Delta E_{lSV} = \frac{1}{\omega}\int_0^{t} v_{lSV} i_{lSV} d(t) =$$
$$\frac{V_{DC} i_{DC}}{6\omega}\left\{\frac{\sqrt{3}}{m_0 \cos\varphi}\left[\cos(\omega t - \varphi) - \cos\varphi\right] - \frac{2}{\sqrt{3}} m_0\left[\cos(\omega t) - 1\right] + \frac{1}{2\cos\varphi}\left[\sin(2\omega t - \varphi) + \sin\varphi\right]\right\} \tag{14}$$
$$+\frac{m_{hSV} V_{DC} i_{DC}}{3\sqrt{3}\omega}\left\{-\frac{\cos(3\omega t) - 1}{3} - \frac{\sqrt{3}}{2m_0 \cos\varphi}\left[\tfrac{1}{2}\sin(2\omega t + \varphi) - \tfrac{1}{4}\sin(4\omega t - \varphi) - \tfrac{3}{4}\sin\varphi\right]\right\}.$$

Similarly, the upper arm energy variation with the sinusoidal modulation is [16]

$$\Delta E_{u0}(\omega t) = \frac{V_{DC} i_{DC}}{6\omega}\left\{-\frac{2}{m_0 \cos\varphi}\left[\cos(\omega t - \varphi) - \cos\varphi\right] + m_0\left[\cos(\omega t) - 1\right] + \frac{1}{2\cos\varphi}\left[\sin(2\omega t - \varphi) + \sin\varphi\right]\right\}. \tag{15}$$

For the test station with parameters listed in Table I, based on (13) and (15), the energy variations per arm are compared in the Fig. 2. The peak-to-peak energy variations per arm with sinusoidal modulation and third harmonic injection are 3.37 MJ and 2.57 MJ, respectively. Thus, with predefined voltage ripple, their SM capacitances are C_{SM0} and $0.76C_{SM0}$, respectively. The SM capacitance with third harmonic injection is reduced by 24%. Compared with sinusoidal modulation, the SM volume, weight, and capital cost are thus lowered by injecting third harmonic.

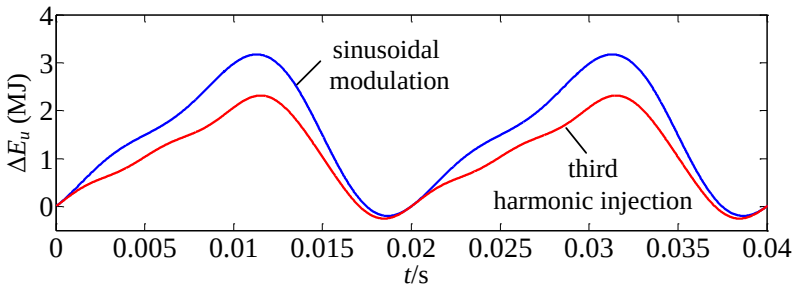

Fig. 2. Energy variations per arm with the sinusoidal modulation and third harmonic injection, for m_0=0.8, V_{DC}=1200 kV, P=1650 MW and φ=0.

C. Circulating Voltages

Assuming SM capacitor voltages in each arm remain balanced, the stored energy in each arm is

$$E_{arm} = \tfrac{1}{2} NC_{SM}\left(\frac{V_{DC}}{N} + \Delta v_{SM}\right)^2 \tag{16}$$

where C_{SM} is the SM capacitance and Δv_{SM} is the SM capacitor voltage ripple. Based on (16), the arm energy variation can be approximated as

$$\Delta E_{arm} = NC_{SM}\left(\frac{V_{DC}}{N} + \Delta v_{SM}\right)\Delta v_{SM} \approx C_{SM}V_{DC}\Delta v_{SM}. \tag{17}$$

Then the SM capacitor voltage ripple can be expressed by the arm energy variation:

$$\Delta v_{SM} = \frac{\Delta E_{arm}}{C_{SM}V_{DC}}. \tag{18}$$

According to (11), (12) and (18) and considering SM capacitor voltage ripple, the upper and lower arm voltages are:

$$v_{uSV} = \tfrac{1}{2}\left(1-\frac{2}{\sqrt{3}}m_0\sin\omega t-\frac{2}{\sqrt{3}}m_{hSV}\sin 3\omega t\right)\left(V_{DC}+\frac{N\Delta E_{uSV}}{C_{SM}V_{DC}}\right) \tag{19}$$

$$v_{lSV} = \tfrac{1}{2}\left(1+\frac{2}{\sqrt{3}}m_0\sin\omega t+\frac{2}{\sqrt{3}}m_{hSV}\sin 3\omega t\right)\left(V_{DC}+\frac{N\Delta E_{lSV}}{C_{SM}V_{DC}}\right). \tag{20}$$

Hence the sum of the upper and lower arm voltages is

$$\begin{aligned} &v_{uSV}+v_{lSV} = V_{DC}+v_{cirSV}+ \\ &\frac{Ni_{DC}\left(m_0\sin\omega t+m_{hSV}\sin 3\omega t\right)}{3\omega C_{SM}}\left\{\frac{\cos(\omega t-\varphi)-\cos\varphi}{m_0\cos\varphi}-\frac{2}{3}m_0\left[\cos(\omega t)-1\right]-\frac{2m_{hSV}}{9}\left[\cos(3\omega t)-1\right]\right\} \end{aligned} \tag{21}$$

where v_{cirSV} is the dominant circulating voltage, specifically

$$v_{cirSV} = \frac{N}{2C_{SM}V_{DC}}\left(\Delta E_{lSV}+\Delta E_{uSV}\right) = \frac{N}{2C_{SM}V_{DC}}\Delta E_{pSV}. \tag{22}$$

According to (13) and (14), the phase energy variation with third harmonic injection is

$$\begin{aligned} &\Delta E_{pSV} = \Delta E_{uSV}+\Delta E_{lSV} \\ &= \frac{V_{DC}i_{DC}}{6\omega\cos\varphi}\left[\sin(2\omega t-\varphi)+\sin\varphi\right]-\frac{m_{hSV}V_{DC}i_{DC}}{3m_0\omega\cos\varphi}\left[\tfrac{1}{2}\sin(2\omega t+\varphi)-\tfrac{1}{4}\sin(4\omega t-\varphi)-\tfrac{3}{4}\sin\varphi\right]. \end{aligned} \tag{23}$$

The phase energy variation with the sinusoidal modulation can be similarly obtained as [16]:

$$\Delta E_{p0} = \frac{V_{DC}i_{DC}}{6\omega\cos\varphi}\left[\sin(2\omega t-\varphi)+\sin\varphi\right]. \tag{24}$$

The circulating current is generated by the circulating voltage, which is imposed on the upper and lower arm inductors and is proportional to the phase energy variation ΔE_{pSV}, depicted by (22). As show in Fig. 3, the phase energy variation is reduced from 1.75 MJ to 1.43 MJ (by around 18.3%) by third harmonic injection. This correspondingly reduces the circulating voltage and thereby benefits circulating current control.

Besides the dominant second component, the fourth component is introduced in the phase energy variation ΔE_{pSV}, due to the third harmonic injection. The phase energy variation is independent of the modulation index and only the third harmonic contributes to phase energy variation reduction.

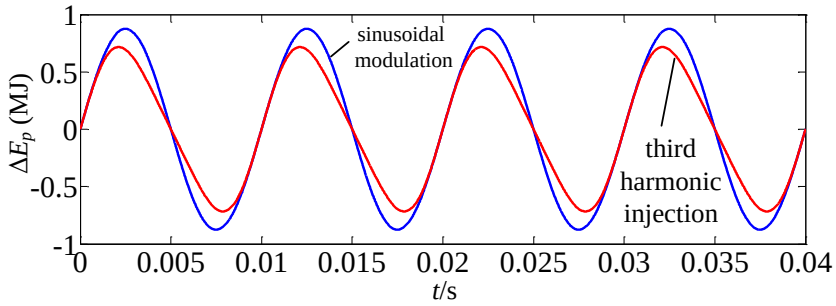

Fig. 3. Energy variations per phase with sinusoidal modulation and third harmonic injection, for m_0=0.8, V_{DC}=1200 kV, P=1650 MW and φ=0 º.

D. Pole-to-Pole DC Fault Currents

A significant challenge with multi-terminal HVDC transmission systems is DC fault protection. In the event of a DC short-circuit, high current flows through the freewheel diodes in the half-bridge MMC, which is currently the preferred HVDC converter configuration, from the AC grid into the fault on the DC-side, even if the station converter is blocked immediately. The low impedance of the short-circuit path leads to a steep rise in fault current which may cause serious damage to the converters and may result in shutdown of the entire HVDC network [4, 21-23]. To limit circulating currents and DC fault currents, the arm inductance L_{arm} is required and can be calculated as:

$$L_{arm} = \alpha \frac{V_{LRMS}^{\ 2}}{\omega P} = \frac{3m^2\eta^2 V_{DC}^{\ 2}}{40\omega P} \tag{25}$$

where V_{LRMS} is the RMS line voltage; P is the rated power; m is the modulation index; α is the pu value of arm inductance, and; η is the DC voltage utilization ratio. With the same arm inductance pu value α, the relationship between arm inductances with sinusoidal modulation and third harmonic injection is derived as (26), according to (25):

$$L_{armSV} = 4/3\, L_{arm0}. \tag{26}$$

Similarly, the converter-side transformer leakage inductance L_{TcSV} increases by a third while the grid-side leakage inductance L_{TgSV} remains unchanged:

$$L_{TcSV} = 4/3\, L_{Tc0}, \qquad L_{TgSV} = L_{Tg0}. \tag{27}$$

Transforming the converter-side inductances to the grid-side, the total AC-side inductance L_{ACSV} with third harmonic injection is the same as with sinusoidal modulation:

$$L_{ACSV} = \frac{L_{armSV} + L_{TcSV}}{n_{SV}^{\,2}} + L_{TgSV} + L_g = \frac{\frac{4}{3}\left(L_{arm0} + L_{Tc0}\right)}{\left(2n_0/\sqrt{3}\right)^2} + L_{Tg0} + L_g$$
$$= \frac{L_{arm0} + L_{Tc0}}{n_0^{\,2}} + L_{Tg0} + L_g = L_{AC0} \tag{28}$$

where L_g is the grid inductance; n_0 and n_{SV} are the transformer ratio for sinusoidal modulation and third harmonic injection respectively. For a pole-to-pole DC fault at the station terminals, which is the most serious fault case for the station, the fault current on the transformer grid-side i_{fgSV} remains unchanged due to the constant grid voltage and the unchanged total AC-side inductance L_{ACSV}, as shown by (28). However, due to the increased transformer ratio n_{SV}, the fault current on the transformer converter-side i_{fcSV} is expected to be reduced by 13.4% by using third harmonic injection, which reduces the current stress on the freewheel diodes and DC circuit breakers, during a DC fault:

$$i_{fcSV} = \frac{i_{fgSV}}{n_{SV}} = \frac{i_{fg0}}{2n_0/\sqrt{3}} = \tfrac{1}{2}\sqrt{3} i_{fc0} = 0.866 i_{fc0}. \tag{29}$$

IV. Simulation Results

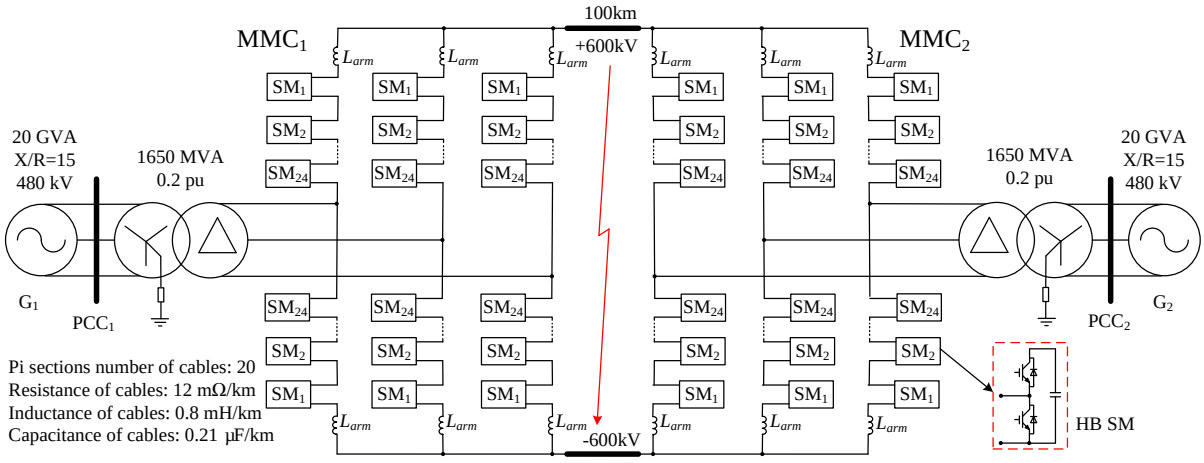

Fig. 4. Point-to-point HVDC link with half-bridge SM based MMCs where N=24.

The MMC performance with third harmonic injection is assessed using a point-to-point HVDC link model as shown in Fig. 4, in the MATLAB/Simulink® environment, where the detailed switching model of the conventional MMC topology with HB SMs is adopted. All the HB SMs are identical and are composed of two IGBTs (including the anti-parallel diodes) and a DC capacitor. The arm inductor L_{arm} is connected in each arm to limit the circulating

currents and the fault currents during a DC fault.

The parameters of the two converters (MMC_1 and MMC_2) are the same, as listed in Table I. In the test system, MMC_1 controls active power exchange with grid G_1 at unity power factor while MMC_2 is configured to regulate the DC link voltage level at ±600 kV, also at unity power factor. A harmonic injection block sets the reference voltages in *abc* coordinates, which has been injected with triplen harmonics, according to (1) and (2). The nearest level modulation is utilized to generate the gating signals [13], based on the outputs of the harmonic injection block.

A. Performances during Normal Operation

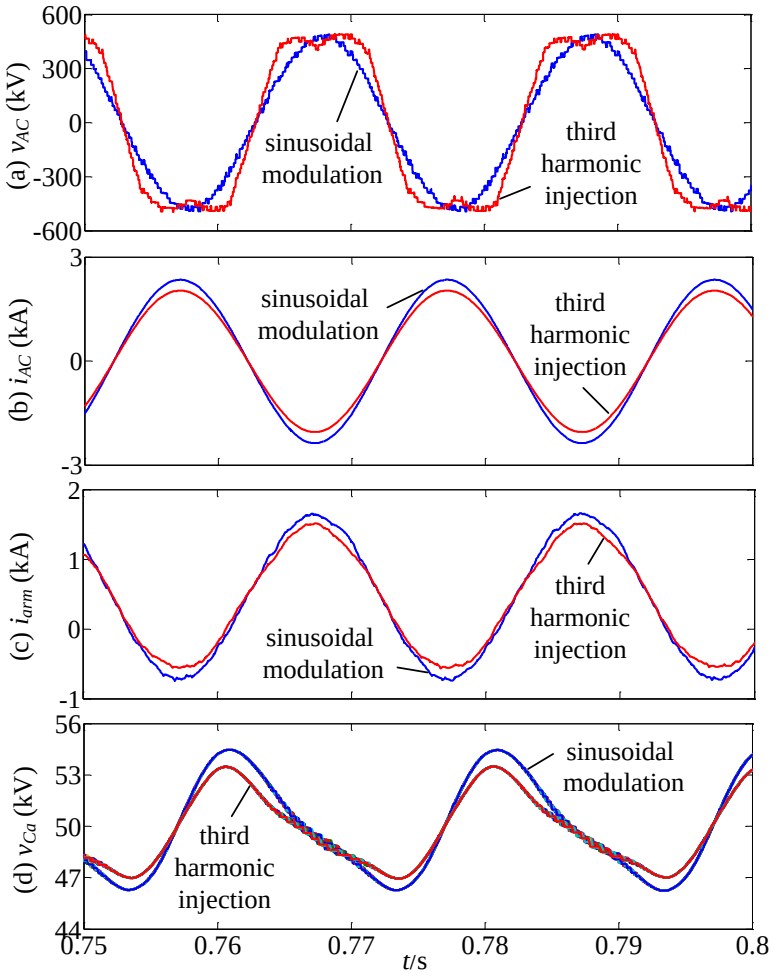

Fig. 5. Comparison between sinusoidal modulation and third harmonic injection in normal operation: (a) AC phase voltages, (b) AC currents, (c) arm currents, and (d) SM capacitor voltages.

The output phase voltages referenced to the mid-point of the DC link are shown in Fig. 5 (a). The voltage peaks with sinusoidal modulation and third harmonic injection are both

controlled around 480 kV. However, benefitting from the injected third harmonic, the fundamental voltage amplitude of the latter is around 554 kV, higher than sinusoidal modulation control (480 kV).

The injected third harmonic only exists in the converter phase voltages and does not affect the quality of the line voltage and current, Fig. 5 (b). With the same transferred power of 1650 MW, the transformer converter-side current peak with third harmonic injection is reduced from about 2.3 kA to 2 kA, as demonstrated in Fig. 5 (b).

As the arm current is the sum of one third the DC current and half the AC current, from Fig. 5 (c), the arm current peaks with third harmonic injection are reduced approximately by 10%, compared with sinusoidal modulation, yielding lower semiconductor current stresses and conduction losses. Fig. 5 (d) shows the simulated SM capacitor voltages. The peak-to-peak ripple with sinusoidal modulation and with third harmonic injection is 8.4 kV and 6.4 kV respectively, which are in good agreement with the calculated values from (15) and (13).

B. Performances during Pole-to-Pole DC Fault

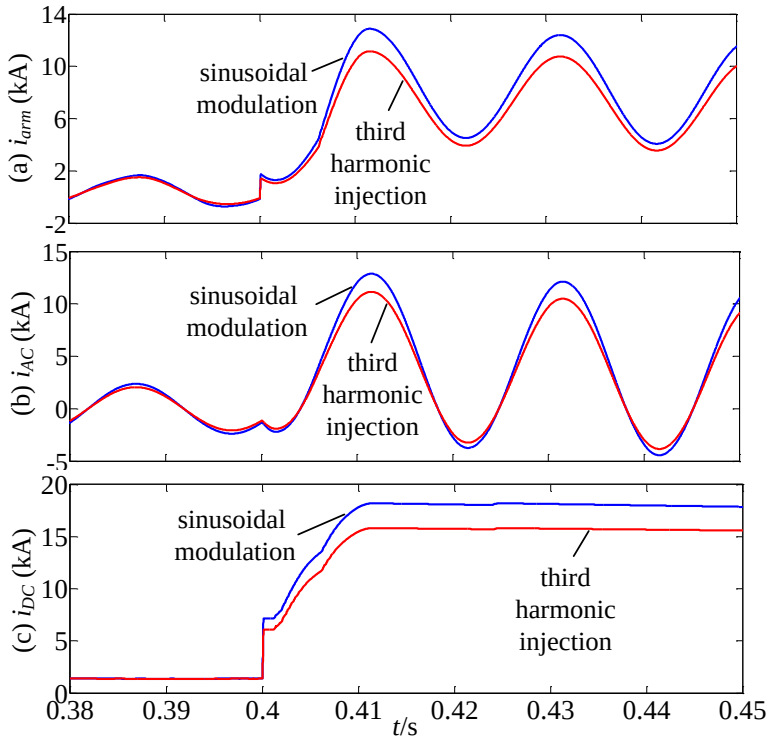

Fig. 6. Comparison between sinusoidal modulation and third harmonic injection during DC fault: (a) arm currents, (b) AC currents, and (c) DC currents.

In this scenario, a permanent pole-to-pole DC fault is applied at the terminals of MMC_1 at t=0.4 s, Fig. 4. Both the stations are blocked after the fault and the circuit breaker action is not considered. As illustrated in Fig. 6 (a), the fault arm current peak is reduced from 12.9 kA to 11.1 kA by using third harmonic injection, yielding lower fault current stresses on freewheel diodes. This is in good agreement with (29). Similarly, the fault DC current peak is reduced by 13.4% and thus the lower capacity DC circuit breakers can potentially be used to isolate the fault, which reduces the capital cost and conduction losses of circuit breakers. In Fig. 6 (b), the fault AC current peaks are also lowered to 86.6% by using third harmonic injection.

Table I summarizes the MMC performance with third harmonic injection. With the same transmitted power (1650 MW), the conduction losses and the SM capacitance are reduced to 89% and 76% respectively, by injecting third harmonic. This significantly improves the system efficiency and reduces the SM volume, weight, and capital cost. Additionally, the DC fault current is expected to be lowered by 13.4%, yielding reduced current stress on freewheel diodes and DC circuit breakers, during a DC fault.

C. Discussion on the Influence of Third Harmonic Injection on AC System

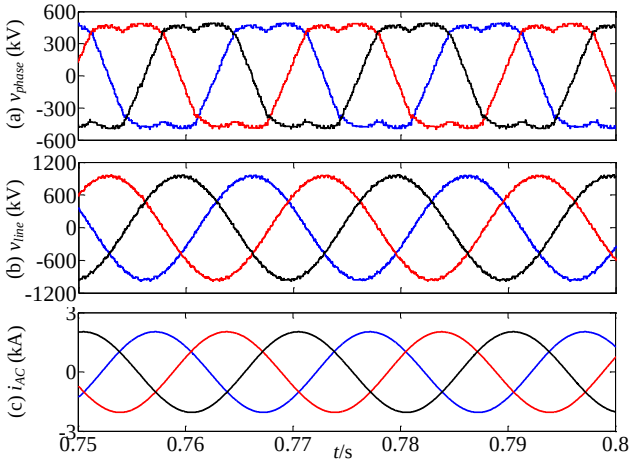

Fig. 7. AC voltages and currents (transformer converter-side) with third harmonic injection: (a) three-phase voltages referenced to the DC-link mid-point, (b) line voltages, and (c) three-phase currents.

The injected third harmonic appears in the phase voltages referenced to the DC-link mid-point, Fig. 7 (a), and the THD of the phase voltage referenced to the DC-link mid-point is high and around 20%, as illustrated in Fig. 8 (a). However, the injected third harmonic is a co-phasal component and is not present in the line voltages or the actual phase voltages, see

Fig. 7 (b). The THD of the line voltage in the test model is thus lower than 3%, as shown in Fig. 8 (b). As a result, the third harmonic does not have negative influence on the quality of the AC-side currents in the HVDC system with Yg/D interface transformer on the AC-side. As displayed in Fig. 7 (c), the three-phase currents are balanced and sinusoidal and do not contain significant third harmonic components.

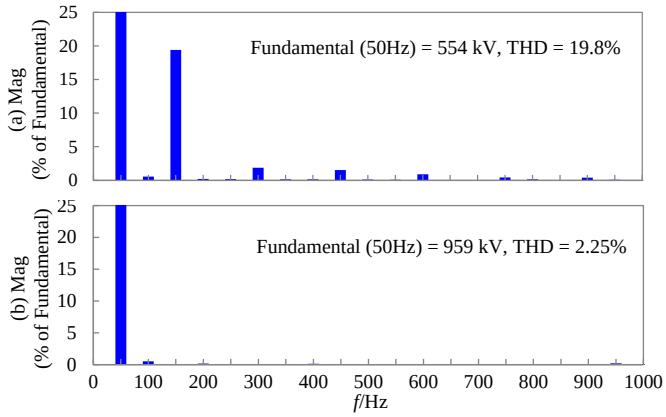

Fig. 8. FFT analysis of: (a) phase voltage referenced to the DC-link mid-point and (b) line voltage.

V. Conclusion

The influences of third harmonic injection on power losses, SM capacitance, circulating current, and DC fault currents are evaluated and the mathematical models are derived. SM capacitance is reduced by 24% compared to that when using sinusoidal modulation, which significantly reduces both the volume and capital cost of SMs. Additionally, station converter conduction losses are reduced by 11% by injecting a third harmonic and the capacity of cooling system is thus reduced. The semiconductor current stresses and phase energy variation are also reduced by using third harmonic injection. Although the converter-side voltage is increased, the DC fault currents are expected to be reduced by 13.4%, yielding lower fault current stresses on semiconductors and DC circuit breakers. Simulation results were in good agreement with the analysis, which demonstrates the effectiveness of the presented models.

VI. Acknowledgments

This work was supported by the Engineering and Physical Sciences Research Council (EPSRC) under Grants EP/K006428/1 and EP/K035096, and the National Natural Science

Foundation of China (NSFC) under Grant 51261130484.

VII. REFERENCES

[1] U. N. Gnanarathna, A. M. Gole, and R. P. Jayasinghe, "Efficient Modeling of Modular Multilevel HVDC Converters (MMC) on Electromagnetic Transient Simulation Programs," *IEEE Trans. Power Del.*, vol. 26, pp. 316-324, 2011.

[2] G. P. Adam, O. Anaya-Lara, G. M. Burt, D. Telford, B. W. Williams, and J. R. McDonald, "Modular multilevel inverter: Pulse width modulation and capacitor balancing technique," *IET. Power Electron.*, vol. 3, pp. 702-715, 2010.

[3] M. A. Perez, S. Bernet, J. Rodriguez, S. Kouro, and R. Lizana, "Circuit Topologies, Modeling, Control Schemes, and Applications of Modular Multilevel Converters," *IEEE Trans. Power Electron.*, vol. 30, pp. 4-17, 2015.

[4] G. P. Adam, K. H. Ahmed, S. J. Finney, K. Bell, and B. W. Williams, "New Breed of Network Fault-Tolerant Voltage-Source-Converter HVDC Transmission System," *IEEE Trans. Power Sys.*, vol. 28, pp. 335-346, 2013.

[5] I. A. Gowaid, G. P. Adam, A. M. Massoud, S. Ahmed, D. Holliday, and B. W. Williams, "Quasi Two-Level Operation of Modular Multilevel Converter for Use in a High-Power DC Transformer With DC Fault Isolation Capability," *IEEE Trans. Power Electron.*, vol. 30, pp. 108-123, 2015.

[6] R. Li, G. P. Adam, D. Holliday, J. E. Fletcher, and B. W. Williams, "Hybrid Cascaded Modular Multilevel Converter With DC Fault Ride-Through Capability for the HVDC Transmission System," *IEEE Trans. Power Del.*, vol. 30, pp. 1853-1862, 2015.

[7] R. Picas, S. Ceballos, J. Pou, J. Zaragoza, G. Konstantinou, and V. G. Agelidis, "Improving capacitor voltage ripples and power losses of modular multilevel converters through discontinuous modulation," in *Industrial Electronics Society, IECON 2013 - 39th Annual Conference of the IEEE*, 2013, pp. 6233-6238.

[8] R. Picas, S. Ceballos, J. Pou, J. Zaragoza, G. Konstantinou, and V. G. Agelidis, "Closed-Loop Discontinuous Modulation Technique for Capacitor Voltage Ripples and Switching Losses Reduction in Modular Multilevel Converters," *IEEE Trans. Power Electron.*, vol. 30, pp. 4714-4725, 2015.

[9] A. Rasic, U. Krebs, H. Leu, and G. Herold, "Optimization of the modular multilevel converters performance using the second harmonic of the module current," in *Power Electronics and Applications, 2009. EPE '09. 13th European Conference on*, 2009, pp. 1-10.

[10] A. Lesnicar and R. Marquardt, "An innovative modular multilevel converter topology suitable for a wide power range," in *Power Tech Conference Proceedings, 2003 IEEE Bologna*, 2003, p. 6 pp. Vol.3.

[11] G. Adam, R. Li, D. Holliday, S. Finney, L. Xu, B. Williams, *et al.*, "Continued Operation of Multi-Terminal HVDC Networks Based on Modular Multilevel Converters," *CIGRE*, pp. 1-8, 2015.

[12] M. Saeedifard and R. Iravani, "Dynamic Performance of a Modular Multilevel Back-to-Back HVDC System," *IEEE Trans. Power Del.*, vol. 25, pp. 2903-2912, 2010.

[13] K. H. Ahmed and G. P. Adam, "New modified staircase modulation and capacitor balancing strategy of 21-level modular multilevel converter for HVDC transmission systems," in *Power Electronics, Machines and Drives (PEMD 2014), 7th IET International Conference on*, 2014, pp. 1-6.

[14] F. Blaabjerg, A. Isidori, and F. M. Rossi, "Impact of modulation strategies on power devices loading for 10 MW multilevel wind power converter," in *Power Electronics for Distributed Generation Systems (PEDG), 2012 3rd IEEE International Symposium on*, 2012, pp. 751-758.

[15] R. Li and D. G. Xu, "Parallel Operation of Full Power Converters in Permanent-Magnet Direct-Drive Wind Power Generation System," *IEEE Trans. Ind. Electron.*, vol. 60, pp. 1619-1629, 2013.

[16] R. Li, J. E. Fletcher, L. Xu, D. Holliday, and B. W. Williams, "A Hybrid Modular Multilevel Converter With Novel Three-Level Cells for DC Fault Blocking Capability," *IEEE Trans. Power Del.*, vol. 30, pp. 2017-2026, 2015.

[17] Q. Tu and Z. Xu, "Power losses evaluation for modular multilevel converter with junction temperature feedback," in *Power and Energy Society General Meeting, 2011 IEEE*, 2011, pp. 1-7.

[18] S. Rohner, S. Bernet, M. Hiller, and R. Sommer, "Modulation, Losses, and Semiconductor Requirements of Modular Multilevel Converters," *IEEE Transactions on Industrial Electronics*, vol. 57, pp. 2633-2642, 2010.

[19] F. B. Ajaei and R. Iravani, "Enhanced Equivalent Model of the Modular Multilevel Converter," *IEEE Trans. Power Del.*, vol. 30, pp. 666-673, 2015.

[20] J. Peralta, H. Saad, S. Dennetiere, J. Mahseredjian, and S. Nguefeu, "Detailed and Averaged Models for a 401-Level MMC-HVDC System," *IEEE Trans. Power Del.*, vol. 27, pp. 1501-1508, 2012.

[21] P. Samuel, R. Gupta, and D. Chandra, "Grid interface of wind power with large split-winding alternator using cascaded multilevel inverter," in *IEEE Trans. Energy Convers* vol. 26, ed, 2011, pp. 299-309.

[22] M. Hamzeh, A. Ghazanfari, H. Mokhtari, and H. Karimi, "Integrating Hybrid Power Source Into an Islanded MV Microgrid Using CHB Multilevel Inverter Under Unbalanced and Nonlinear Load Conditions," *IEEE Trans. Energy Convers*, vol. 28, pp. 643-651, 2013.

[23] S. Debnath, Q. Jiangchao, B. Bahrani, M. Saeedifard, and P. Barbosa, "Operation, Control, and Applications of the Modular Multilevel Converter: A Review," *IEEE Trans. Power Electron.*, vol. 30, pp. 37-53, 2015.